This is a postprint of an article already published. The final authenticated version is available online at:
Brouwers LB, Dippenaar MA (2018). Partially saturated flow from sand into a discrete smooth open vertical fracture at the soil–rock interface: experimental studies. Bulletin of Engineering Geology and the Environment. https://doi.org/10.1007/s10064-018-1258-x

Partially saturated flow from sand into a discrete smooth open vertical fracture at the soil-rock interface: experimental studies

Luke B. Brouwers[1] & Matthys A. Dippenaar[1a]

[1] Engineering Geology and Hydrogeology, Geology Department, University of Pretoria, South Africa

[a] Corresponding author: matthys.dippenaar@up.ac.za / madippenaar@gmail.com

Abstract

The two proposed conceptual models explaining partially saturated flow from soil into fractured rock in the intermediate fractured vadose zone have not been confirmed due to difficulty in observing the soil-rock interface in-situ. To combat this challenge, this paper presents a series of newly developed physical experiments using a geotechnical centrifuge model of sand overlying a single dry clean smooth vertical fracture. The model shows the development of a perched water system and saturated wetting front progressing transversely along the interface, while breaching through the interface occurs as multiple point sources. The dominant flow mechanisms within the fracture comprise of droplets, discontinuous rivulets with droplet formation, and continuous rivulets. A maximum value of 30% drainage area within the fracture contributes to flow in the model which decreases with depth due to merging of oscillating rivulets in the upper regions of the fracture. The supporting evidence for the two conceptual models shows that a combined conceptual model is required to accurately explain partially saturated flow at the soil-rock interface.

Keywords: Physical Modelling; Soil-Rock Interface; Variable Saturation; Fracture Flow; Flow Mechanisms; Geotechnical Centrifuge

1. Introduction

The vadose zone – situated between land surface and the phreatic surface or groundwater table – is comprised of soil and rock and, as water flows from soil to rock, it progresses from flow between pores to flow within fractures. The soil-rock interface is an important factor for seepage through the vadose

zone with overlying material (i.e. saprolite) above the fractured bedrock hydraulically linking the different systems (Nimmo 2005; Kosugi et al. 2006). This has important influences on, for instance, slope stability, contaminant transport, waste disposal, groundwater recharge, interflow systems, the occurrence of perched water systems and ephemeral springs. Research on the vadose zone comprises of field and numerical studies, with numerous researchers observing characteristic flow features above the soil-rock interface including transient perched water systems, remnant fractures in the saprolite forming preferential flow feeding pathways, lateral preferential flow along the interface, localised areas of bedrock discharge and diffusion of moisture contents between infiltration events (e.g. Appels et al. 2015; Boisson et al. 2015; Buttle and McDonald 2002; Dippenaar 2014a; Dippenaar 2014b; Fujimoto et al. 2014; Graham et al. 2010; Huang et al. 2015; Liang and Uchida 2014; Masaoka et al. 2010; Sohrt et al. 2014; Salve et al. 2012; Tromp-van Meerveld and McDonnell 2006).

However, the flow mechanisms active within the two systems differ; furthermore, focus on the flow transition from soil into rock is poorly explained and limited to a handful of studies (e.g. Banks et al. 2009; Boisson et al. 2015; Faybishenko et al. 2000; Greco et al. 2014; Kosugi et al. 2006; Preuss 1999; Salve et al. 2012). Presently there are two proposed conceptual models of water flow through the soil-rock interface where: (1) fractures behave as capillary barriers; or (2) fractures promote film flow (Hsieh et al, 2001). Research investigating these proposals is constricted to numerical methods (Kordilla et al. 2013; Lebeau and Konrad 2010; Peters and Durner 2008; Tuller and Or 2002; Zhang 2011), due to the inability to access the soil-rock interface without disturbing in-situ properties.

Engineering and infrastructure development is notably affected by the storage and movement of water at the soil-rock interface. This is exacerbated by inducing change to the natural conditions, and it becomes important to be able to anticipate subsurface hydrological changes during the project life cycle. The soil-rock interface governs the occurrence of perched water and shallow interflow systems and defines where and how deeper percolation to eventual recharge of the groundwater system will occur. In imposing change on a natural system, it is no longer good enough to know that ground is occasionally wet. Instead, it is necessary to understand how flow occurs at partial saturation, what the influence of this unsaturated state would be on the integrity of infrastructure due to wetting or drying of

ground, and then to anticipate, for instance, how this will affect corrosivity of site materials to cement, steel and other manmade materials.

This paper presents a set of soil-rock interface experiments using a geotechnical centrifuge that is able to replicate in-situ conditions to evaluate the two conceptual models for partially saturated flow at the soil-rock interface. A controlled influx is introduced to a hypothetical scenario of uniform sand overlying a discrete clean smooth vertical fracture with parallel walls. The main research aims are to (i) physically observe the flow transition from soil into the fracture as well as the flow mechanisms within the fracture, providing a unique viewpoint currently missing within vadose zone research and (ii) address the validity of the two current conceptual models for partially saturated flow at the soil-rock interface. In establishing the behaviour of water at the soil-rock interface under controlled experimental conditions, follow-up efforts can focus on expanding the knowledge gained to more complex and natural systems.

2. Literature

2.1. Unsaturated Fracture Flow

The first conceptual model for partially saturated flow in fractures considered flow mainly occurring through the matrix (Wang and Narasimhan 1993 in Singhal and Gupta 2010). However, this model failed to explain how fast flow could occur within fractures and was subsequently superseded by the film flow conceptual model proposed by Tokunaga and Wan (1997). This latter model occurs as thin films of water flowing along the fracture surface without having to fully saturate the fracture, with the hydraulic conductivity of the film related to film thickness (which, in turn, is related to the degree of saturation where an increase in saturation results in thicker films). The boundaries for film flow to occur in unsaturated rocks are a matrix permeability less than 10^{-14} m^2 and aperture width greater than 30 μm that covers a large range of unsaturated rocks (Tokunaga and Wan 2001). Research by Or and Tuller (2000), Dragila and Wheatcraft (2001) and Nimmo (2010) support the experimental findings of Tokunaga and Wan (1997) and show that film contribution in unsaturated conditions is not negligible.

Doe (2001) highlights that film flow considers scenarios where there is sufficient water supply and the material exhibits a contact angle of zero. Therefore, for scenarios outside these boundaries, a droplet flow conceptual model is explored by Doe (2001) and incorporates single wall (drops) and double wall (liquid bridges) features. Further additions to the film flow and droplet flow conceptual models is provided by Su et al. (1999) who define a separate flow mechanism known as rivulets where a continuous tendril of water wets both fracture walls simultaneously. The existing rivulets depend on aperture and, depending on the flow rate into the fracture, three possible scenarios can occur (Su et al. 1999):

- At low flow rates, continuously snapping rivulets form liquid bridges within the fracture.
- At medium flow rates, rivulets form and only snap at the fracture's end.
- At high flow rates, the rivulets formed are maintained throughout the fracture.

Dragila and Weisbrod (2003) obtained similar results and added that the rivulets contributed to droplet formation, with longer contact time supplying larger droplets and the possibility for droplets to travel faster than film flow in unsaturated conditions. Further research by Or and Ghezzehei (2007) shows that the interaction of liquid bridges with fracture walls could supply complex travel velocity-distance relationships due to the formation and detachment of liquid bridges within unsaturated fractures.

The different flow regimes and wetting front instabilities present are dependent on the interplay between gravitational (body), capillary (surface tension) and viscous forces (Or 2008). The importance of these forces can be quantified by dimensionless quantities shown in Table 1 where the Reynolds Number represents the influence of inertial to viscous forces; the Bond Number the effect of gravitational to capillarity forces; and the Capillary Number the relative effect of viscous to capillary forces acting along an interface between two fluids. Our current inability to accurately capture film and capillary force interactions leads Ghezzehei (2004) to conclude that a prominent conceptual model is difficult to obtain as a multitude of different flow regimes are able to occur simultaneously within fractures.

Table 1 - Commonly used dimensionless quantities

Dimensionless quantities	Equation	Relationship	Variables
Reynolds Number	$R_e = \rho vL/\mu$	*Inertial :* *Viscous*	ρ - *density* *v - velocity* σ - *surface tension* μ - *dynamic viscosity* *L - characteristic length* *g - gravitational acceleration*
Capillary Number	$Ca = \mu v/\sigma$	*Viscous :* *Capillary*	
Bond Number	$Bo = \Delta\rho gL^2/\sigma$	*Gravitational :* *Capillary*	

2.2. Centrifuge Modelling

A geotechnical centrifuge offers a powerful physical modelling technique that is capable of replicating gravitational dependent processes between a scaled model and prototype conditions (Phillips 1995; Taylor 1995). The fundamental basis of geotechnical centrifuge modelling requires that the stress and strain conditions are identical between the scaled model and prototype. To achieve this similitude, the geometric, kinematic and dynamic properties can be scaled by selecting a rotational speed that induces an artificial gravity that is N times stronger than Earths' gravity (g) within the model compared to the prototype, ensuring a constant ratio between dimensions, forces, velocities and accelerations (Butterfield 2000; Garnier et al. 2007; Kumar 2007).

Geotechincal centrifuge modelling uses Darcy's Law to evaluate seepage where the seepage velocities, and subsequently the Reynolds Number, are scaled by a factor of $1/N$ (Culligan-Hensley and Savvidou 1995). Even if the Reynolds Number between the model and Prototype are not identical, similitude in behavior is maintained, provided the Reynolds Number remains less than 10. There is currently some controversy behind how the scaling factor for seepage velocity is determined, with the debate focusing on two main factors namely: the interpretation of hydraulic gradient and permeability in Darcy's equation (Taylor 1995). Research by Jones et al. (2017a), Jones et al. (2017b) and Van Tonder and

Jacobsz (2017) indicates that permeability remains constant while the hydraulic gradient is scaled by a factor of N.

When performing flow scenarios in a geotechnical centrifuge, time is also scaled with a scaling factor of N^2 (Taylor 1995). This scaling factor can be easily deduced by considering the distance of travel scales as N and the speed of travel scales as $1/N$. This simple dimensional analysis can be extended to derive the remaining basic scaling factors used in geotechnical centrifuge modeling as shown in Table 2.

Table 2 - Geotechnical centrifuge scaling factors (Taylor, 1995; Culligan and Barry, 1998; Garnier et al, 2007)

Parameter	Symbol	Prototype/Model ratio
Gravity	g	$1/N$
Macroscopic length (i.e. soil height)	l	N
Microscopic length (i.e. fracture aperture)	l	1
Stress	σ	1
Strain	ε	1
Mass	m	N^3
Force	F	N^2
Dynamic viscosity	μ	1
Intrinsic permeability	κ	1
Density	ρ	1
Seepage velocity	v	$1/N$
Time	t	N^2
Reynolds number	R_e	$1/N$

In a qualitative study as presented here, and although scaling of the Reynolds Number is known to be 1/N, calculation of the Reynolds, Capillary and Bond Numbers (Table 1) were excluded as (i) numbers will likely be misleading and based on estimation of flow velocities and characteristic lengths at best,

and (ii) scaling of parameters involved in quantification of these numbers may contribute unwanted inaccuracy. The authors therefore decided to keep this study purely qualitative until limitations are known to move towards quantitative studies.

3. Materials and Methods

3.1. Soil and Geosynthetic Material

The model uses uniform, clean, poorly-graded, oven dried sand with an average particle size of 135 μm (Archer 2014). A grading curve of the sand is shown in Figure 1 and the sand exhibits an average hydraulic conductivity of 1.6 x 10^{-5} m/s. A geosynthetic material is used to limit the interference of the sand and the clean fracture by providing a thin barrier between the two components while maintaining hydraulic properties similar to the overlying sand. A nonwoven needle-punched continuous filament polyester geotextile known as BIDIM A2 exhibiting an average pore size of 170 μm and an average hydraulic conductivity of 4.2 x 10^{-3} m/s (Kaytech 2014) is selected to achieve this purpose.

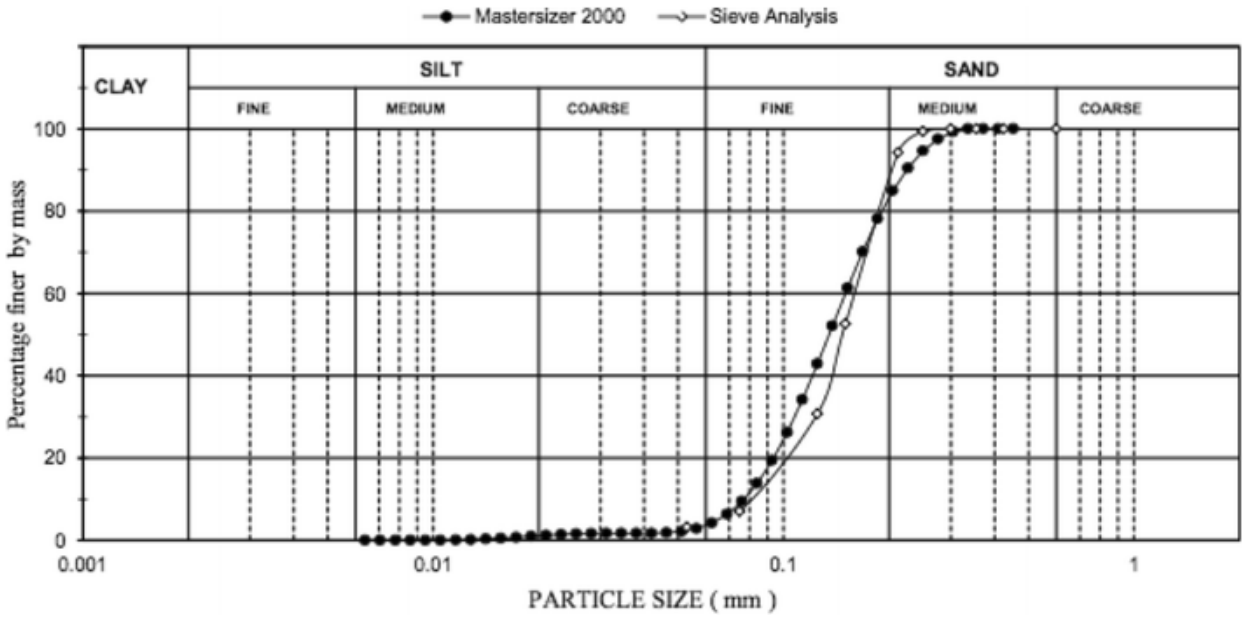

Figure 1 - Particle size distribution curve for sand used in geotechnical model (Archer, 2014).

3.2. Fracture Material

Two acrylic sheets are used to represent the vertical fracture due to the materials' transparency, machinability and homogeneous surface which exhibits an average contact angle of ca. 70° (Della Volpe et al. 2002). The dimensions (length x width x thickness) for the sheets are 400 x 150 x 10 mm and 399 x 150 x 10 mm respectively. Both sheets are bent 90° at a distance of 100 mm from the edge to form a vertically dipping fracture. Two semicircles, with diameter of 30 mm, are drilled at the base of the fracture, spaced at 30 mm intervals, to ensure free drainage conditions at the bottom of the fracture. The completed fracture assembly shown in Figure 2 shows the geosynthetic material in the center covering a 1mm aperture secured by masking white tape and foam insulation tape along the perimeter edge of the acrylic sheets to ensure a water tight seal.

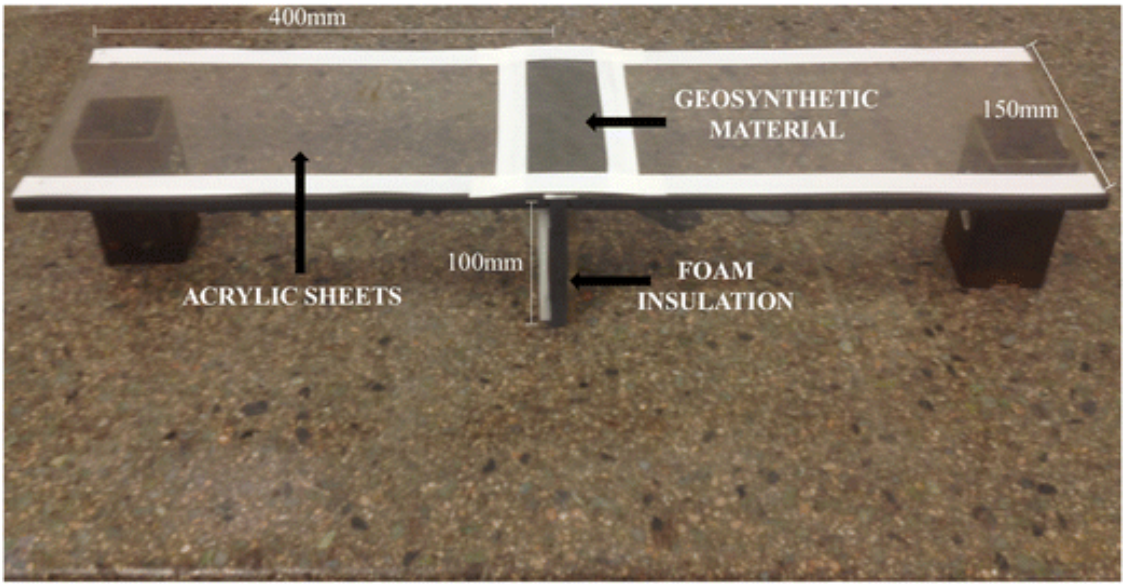

Figure 2 - Completed Acrylic sheets fracture set up

3.3. Centrifuge Model

A 150 G-ton Actidyn C67-4 geotechnical centrifuge with a 3 m arm radius housed at the Department of Civil Engineering at University of Pretoria is used for the experiments (Jacobsz et al. 2014). A schematic of the completed geotechnical centrifuge model constructed in a windowed strongbox is shown in Figure 3.

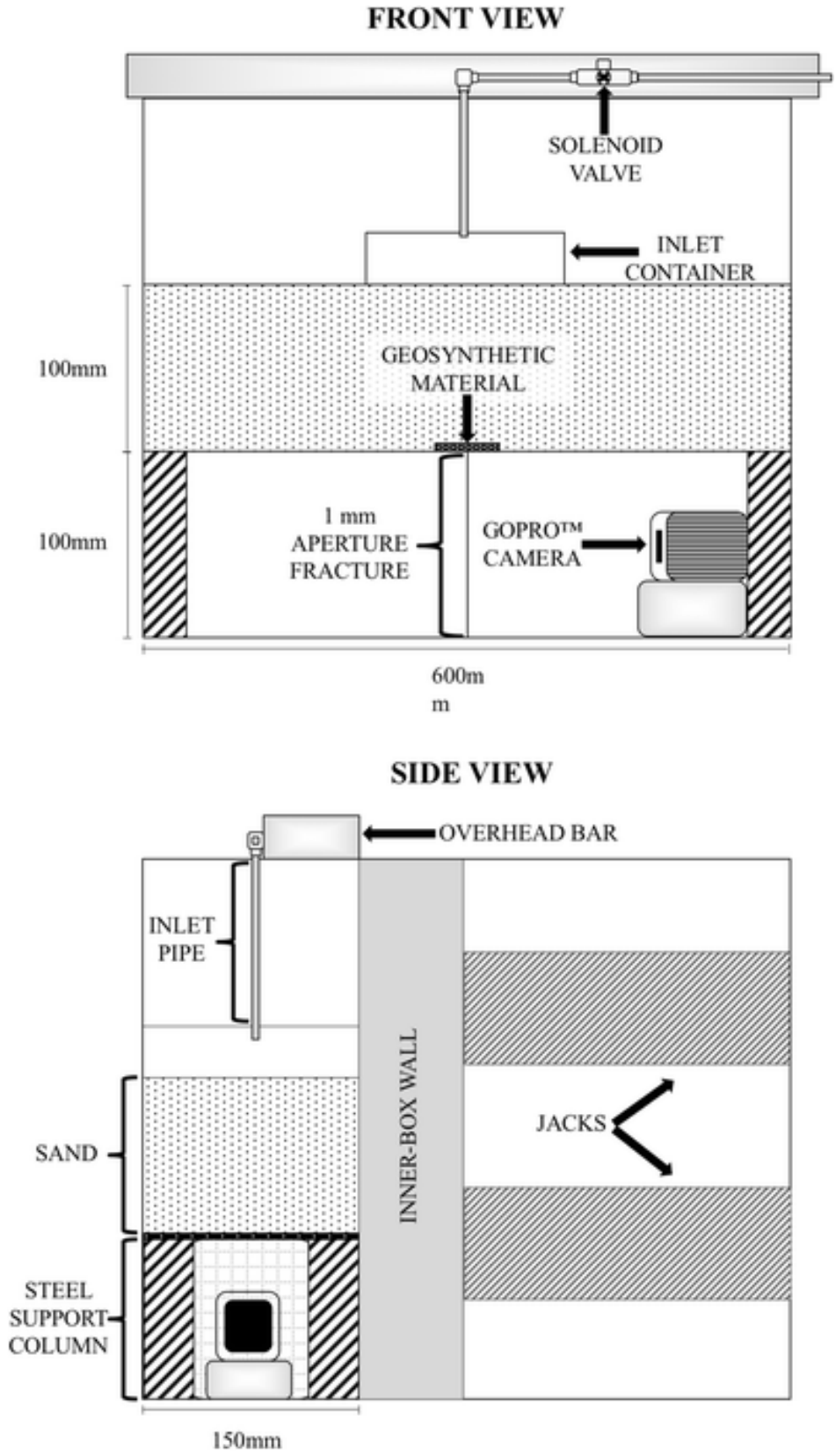

Figure 3 - Geotechnical centrifuge model schematic for soil-rock interface experimental studies.

Model preparation is completed using the following steps:

i. Clean uniform, poorly-graded sand and acrylic sheets are oven dried over night at 60 °C.

ii. A transparent square grid is positioned on one fracture wall exterior by insulation tape.

iii. The acrylic sheets are placed together with 1 mm separation-spacers to maintain a constant 1 mm aperture.

iv. Foam insulation tape is installed around the perimeter of the acrylic sheets to maintain a watertight seal once confined.

v. A thin BIDIM strip is placed above the fracture and fastened by insulation tape.

vi. Four metal support columns with dimensions 50 x 50 x 90 mm are placed into the corners of the strongbox to stop rotation of the fracture set during placement of the overlying sand.

vii. A Go-Pro™ Hero session is placed on a raised platform between the columns.

viii. The fracture set is placed on top of the support columns.

ix. An aluminum back plate is installed with three turnbuckle jacks to create a watertight seal for the fracture set against the window and the back plate.

x. The model's weight is recorded before and after pluviating clean dry sand over the fracture set by a mechanical hopper with a 2 mm slit, from a height of 0,75 m to ensure a constant density range between 1600 kg/m^3 and 1700 kg/m^3.

xi. A water inlet container, with a 2 mm wide slit lined with BIDIM and potassium permanganate crystals, is placed in the center on top of the sand.

xii. An overhead bar with a water inlet pipe, connected to solenoid valves, is installed.

xiii. An outlet drainage pipe is connected to a waste water storage tank in the base of the model.

xiv. LED lights and a remotely operated camera are installed on the exterior of the strongbox.

3.4. Experimental Procedure

Two experiments are conducted, at two different acceleration levels, and with a continuous influx of water being introduced remotely using solenoid valves. The first experiment is performed under no acceleration (i.e. 1g) to develop a comparison for the accelerated experiment. The following procedure is followed in the 1g experiment:

i. Water is introduced at an influx of 20 l/hr for a total of 20 minutes.

ii. The influx is stopped and the model is allowed to drain for 20 minutes.

iii. Water is reintroduced at an influx of 20 l/hr for a total of 5 minutes.

iv. The influx is stopped and the model is allowed to drain for 5 minutes.

v. The model is dismantled, wet sand is discarded and the acrylic sheets are washed with distilled water before repeating model preparation for the next experiment.

The newly constructed model is then accelerated to 20g acceleration level at 77.23 rpm (rotations per minute) at a 3 m radius to replicate a prototype scenario with 2 m of sand overburden on top of a 2 m long and 2 m wide discrete fracture with a 1 mm aperture. Upon stabilising at the required acceleration level, the following procedure is followed:

i. Water is introduced at an influx of 20 l/hr for a total of 5 minutes.

ii. The influx is then stopped and the model is allowed to drain for 5 minutes.

iii. Water is reintroduced as droplets at 1 l/hr for a total of 10 minutes.

iv. The influx is then stopped and the model is allowed to drain for a total of 10 minutes.

4. Results and discussion

4.1. Dispersion Plume

Timed images of the front view of the model, taken by the exterior web camera, detail the evolution sequence of the dispersion plume formed during the 1g (Figure 4 A-I) and 20g (Figure 4 a-i) experiments. The top third of the image shows the white water inlet container centred on top of the sand. This sand rests on top of the vertical fracture, which occupies the lower third of the image where a Go-Pro™ camera, offering a fracture view, can be seen in the lower right segment of each image.

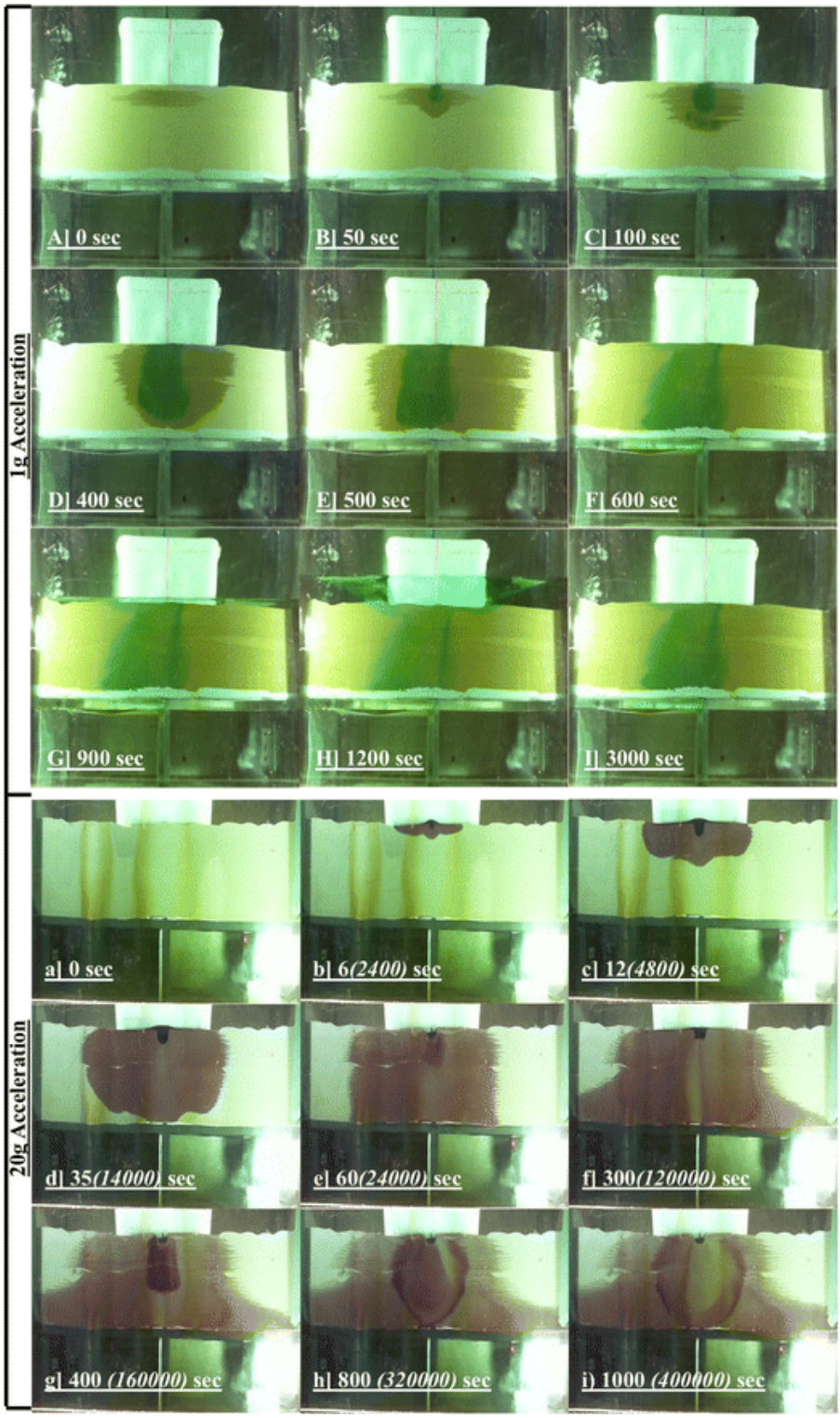

Figure 4 - Front view of 1g (A-I) and 20g (a-i) experiments dispersion plume evolution with prototype conditions represented in brackets

During the 1g experiment, the dispersion plume begins to spread as a circular wetting front attempting to saturate as much of the sand as possible before contacting the soil-rock interface (Figure 4 A-D). At this stage the dispersion plume begins to spread laterally and saturate all of the sand, developing a perched system that gradually rises above the top of the sand as seen by the coloured water above the sand (Figure 4 H). After the water supply is stopped, the perched system gradually lowers until it is no longer visible above the surface (Figure 4 I).

During the 20g experiment, the dispersion plume initially spreads to a width of 200 mm where it then progresses through the sand with an almost linear wetting front (Figure 4 a-d). The dispersion plume continues to migrate through the sand until contacting the soil-rock interface where it begins to spread to form a large bell shape (Figure 4 e-f). This indicates the presence of a capillary barrier despite the disappearance of the water table above the sand when compared to the 1g experiment. This capillary barrier correlates to the development of observed field implications such as transient saturated areas, lateral preferential flow, perched water systems and redistribution of moisture contents (e.g. Buttle and McDonald 2002; Fujimoto et al. 2014; Huang et al. 2015; Liang and Uchida 2014; Masaoka et al. 2010; Sohrt et al. 2014).

Halting the water supply results in a separate smaller interior 'drying' column within the initial plume that becomes stationary 50 mm below the sand surface as the remaining water drains through the sand (Figure 4 g). This indicates that the maximum influx entry into the fracture is dependent on the overlying materials' hydraulic conductivity. Re-addition of water causes bulging and spreading of the static drying plume in a circular fashion (Figure 4 h). The new water occupies the interior of the circle and only a small proportion of the original dispersion plume encounters the soil-rock interface (Figure 4 i). This indicates the possibility for contaminants to be trapped within the soil profile for prolonged periods as each new saturating event causes the previous plumes' progression to spread outwards, omitting the majority of the previous plume from contacting the interface.

4.2. Soil to vertical Fracture

The positioning of the camera within the hollowed section of the bent acrylic sheets allows for a unique viewpoint of the soil-rock interface. For the 1g experiment, the view shows the overlying sand as a brown colour in the top third of the image. The grey 1 mm separation spacers can be viewed on either side of the fracture and runs for the entire 100 mm length of the fracture. Flow observation and analysis is confined to the 10 x 10 mm grid area between the separation-spacers, resulting in a fracture width of 110 mm.

A similar view is obtained for the 20g experiment; however the 1 mm separation-spacers are now white in colour. There is also a reflection of the 5 x 5 mm grid along the interface in the top portions of the images; however, the soil-rock interface can still be seen by the appearance of a thin horizontal grey line within the image. Similarly, flow observations and analysis are confined to the grid area between the separation spacers. Zoomed-in images are also presented within this section to highlight and detail specific flow phenomena observed within the fracture. In these zoomed images, the soil-rock interface occurs directly at the top of the images or can be easily deduced from colour difference between the two media at the interface.

4.2.1. Breaching

As the water contacts the soil-rock interface it begins to spread along the interface as outlined in Figure 5a. Breaching into the fracture occurs at 222 seconds as a single droplet, 15 mm from the right separation spacer (Figure 5b). A continuous stream follows the progression of the droplet, where two possible generic scenarios occur:

i. A droplet with sufficient volume progresses through the fracture without disconnecting from the stream and a continuous rivulet is formed in one breach event (Figure 6a-b).
ii. A droplet disconnects from the stream and progresses as a single self-contained droplet, while a new droplet forms at a discontinuous rivulet (Figure 6c). This process repeats and progresses the discontinuous rivulet further down the fracture, thereby increasing the total length (Figure 6d) until the formation of a continuous rivulet.

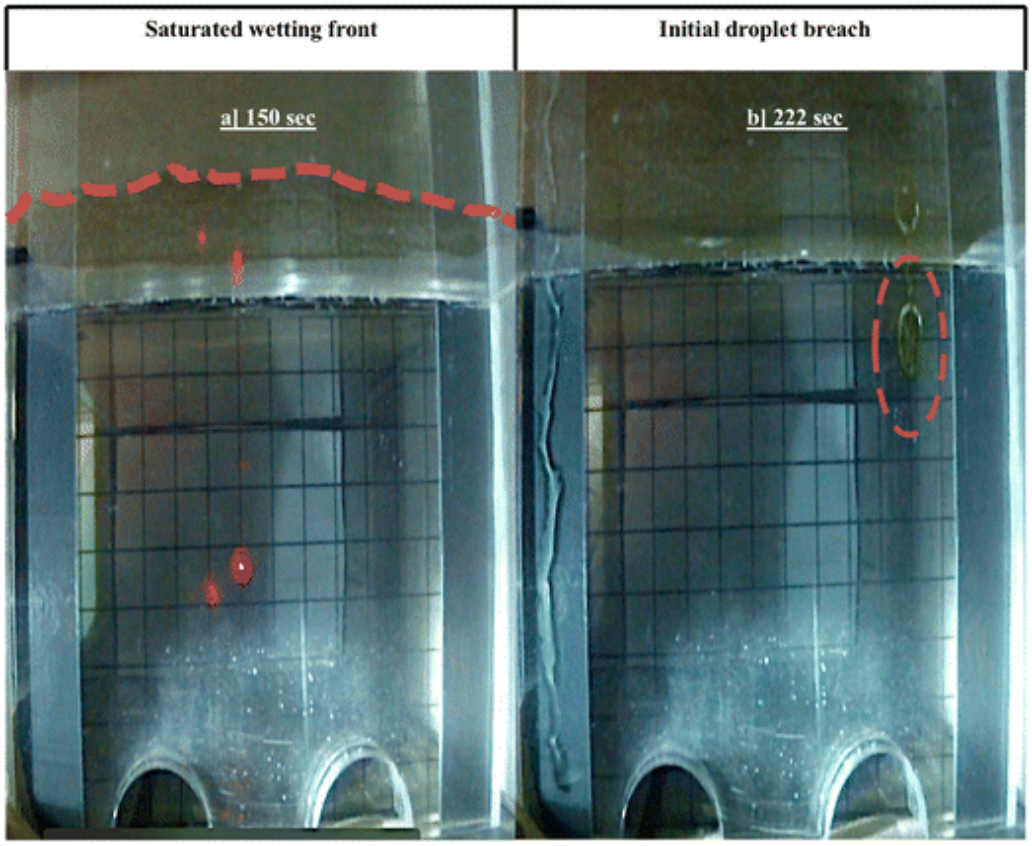

Figure 5 - Fracture view of 1g experiment–initial breaching through the interface, where a saturated wetting front is outlined in (a) and initial breach locality marked by a circle in (b).

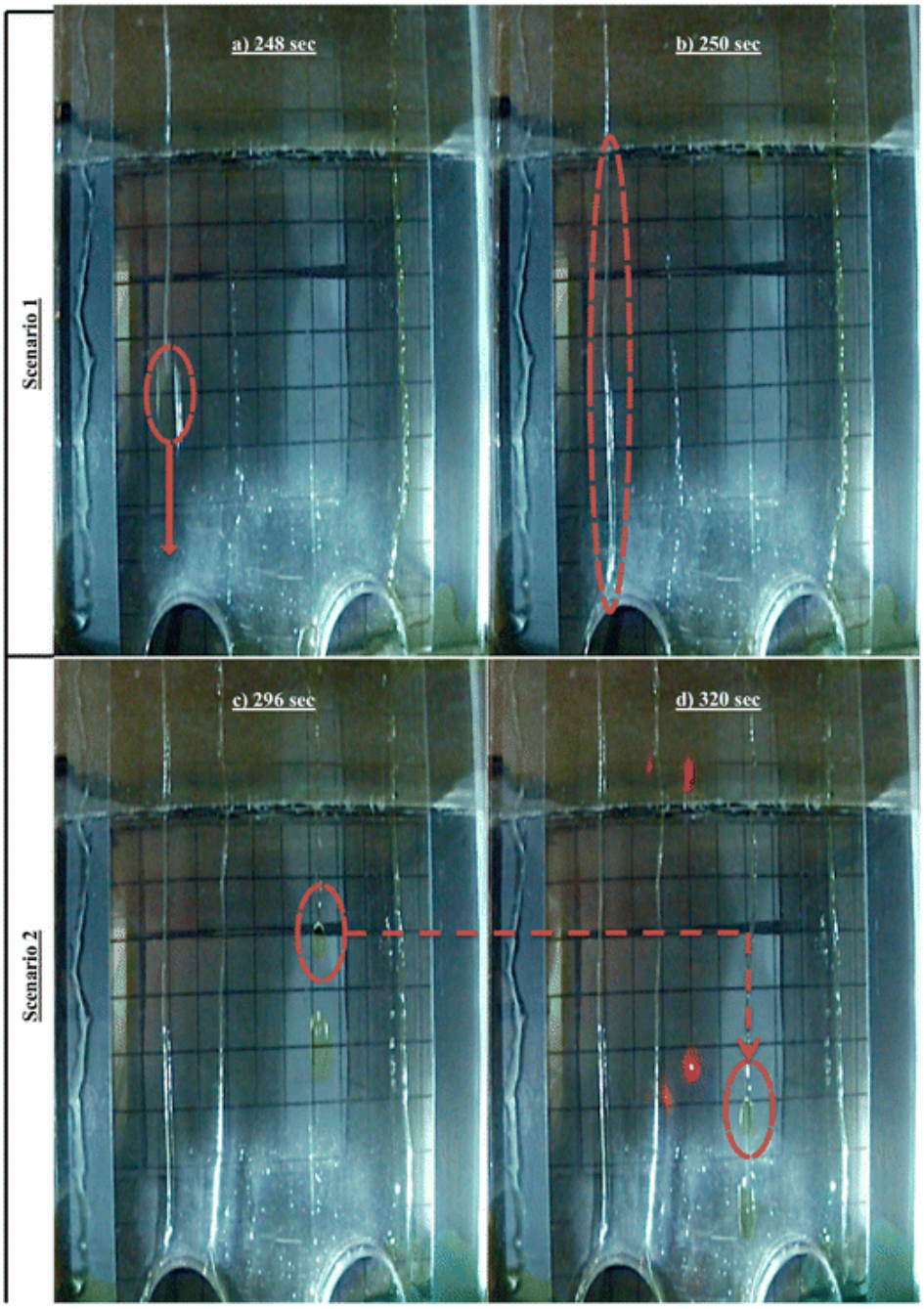

Figure 6 - Fracture view of two possible breaching scenarios observed in 1g experiment: (a-b) full continuous rivulet establishment from single droplet breach; (c-d) discontinuous rivulet with droplet formation progressing down fracture

The breaching through the interface for the 1g experiment mimics the findings by Nicholl et al. (1994), Su et al. (1999) and Dragila and Weisbrod (2003) where initially breaches occur as individual droplets that create wetted paths for discontinuous rivulets with droplet formation to develop. Ultimately, the discontinuous rivulets progress down the fracture and form fully maintained continuous rivulet within the fracture.

The 20g experiment exhibits identical breaching methods through the interface despite the increased hydraulic gradient. After 32 (*12800, in prototype*) seconds of water addition, the initial breach occurs while no saturated front along the interface can be seen. The initial breach occurs as a droplet with sufficient volume to maintain a rivulet throughout the 100 (*2000*) mm length of the fracture (Figure 7a-c). This is quickly followed by a second rivulet, which breaches and connects to the first rivulet 45 (*900*) mm from the base of the model (Figure 7d-e). The coloured stain apparent in right portions of Figure 7 represents water flowing between the separation spacer fracture surface, although this area is not within the defined analysis region. It may highlight the importance of aperture and contact points to variably saturated flow through fractures as discussed by Dippenaar and Van Rooy (2016).

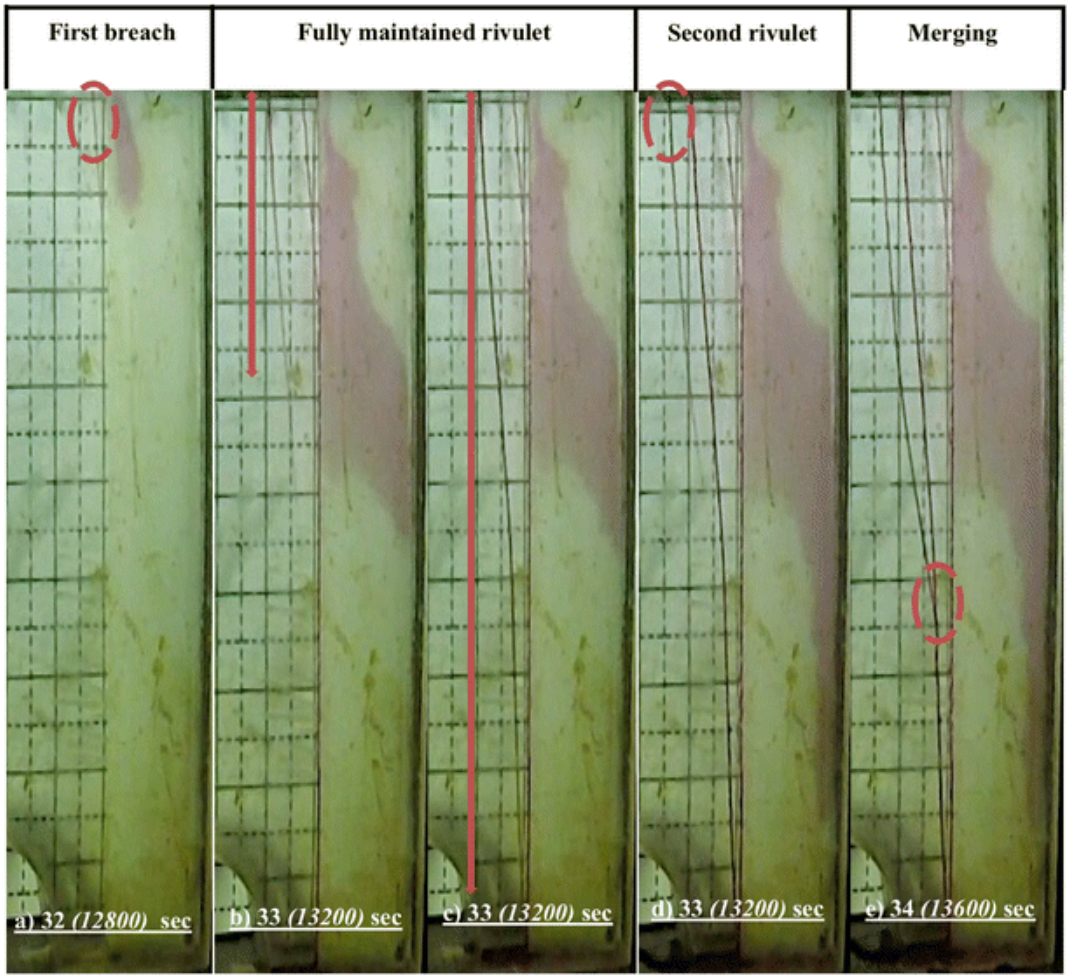

Figure 7 - Fracture view screenshots of initial breaching progression into the fracture for the 20g experiment, with circles representing breach localities or merging points; and arrows illustrating length of rivulet.

4.2.2. Flow mechanisms

During initial wetting of the 1g experiment, multiple breaches occur sporadically through the soil-rock interface at different locations along the interface (Figure 8a). Similarly, in the 20g experiment, the breaching process occurs as multiple point sources through the interface (Figure 8c). The multiple preferential point sources are located where initial breaching through the capillary barrier occurs, which subsequently lowers the invasion pressure required for subsequent breaching at this point. This process may be amplified by the preferential feeding channels in overlying material as stated by Salve et al. (2012) and Boisson et al. (2015).

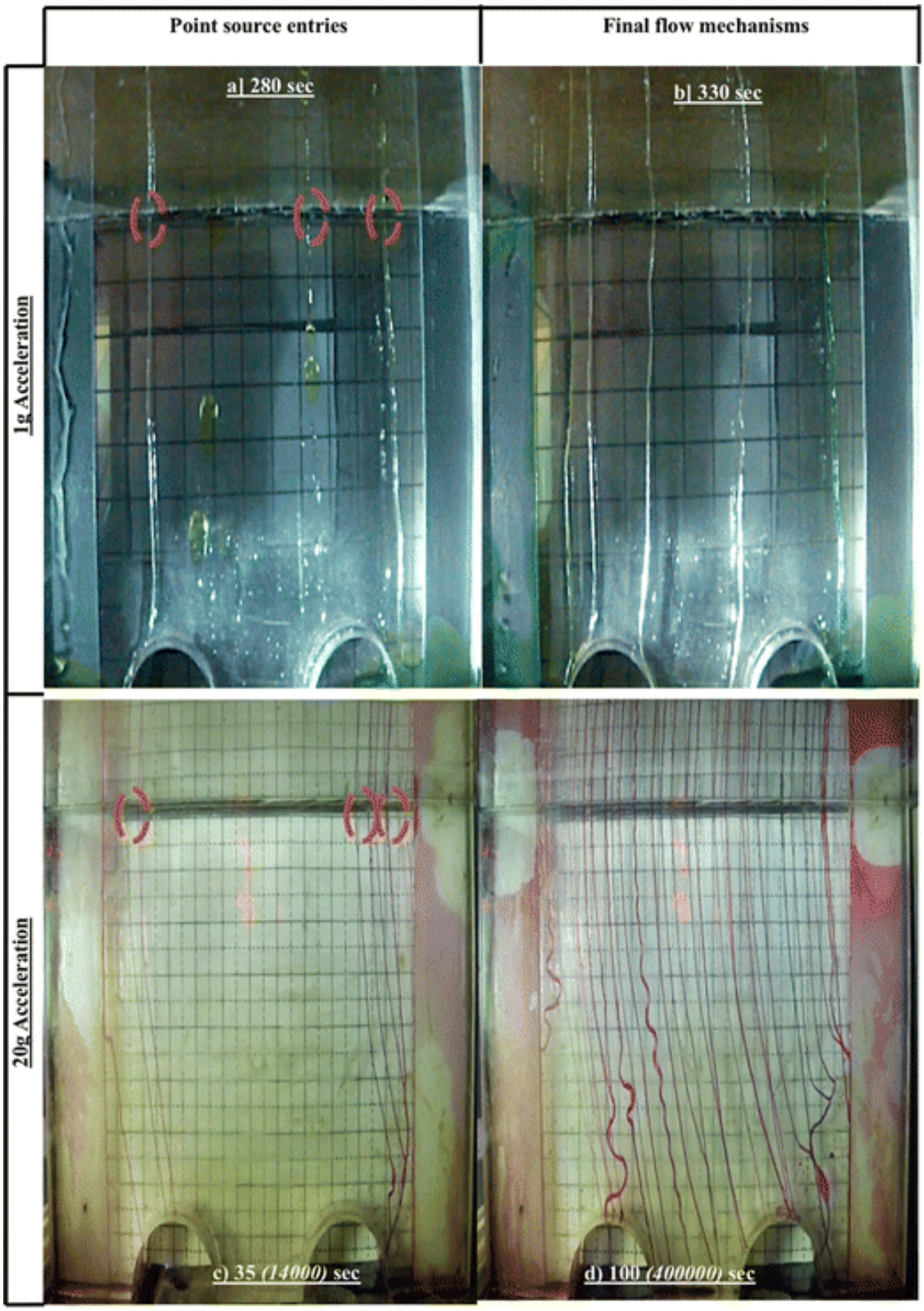

Figure 8 - Fracture view illustrating point source localities marked by circles and final flow mechanisms established within the fracture for 1g (a-b) and 20g (c-d) experiments.

During the 1g experiment, the final flow mechanisms comprises a set number of separate individual continuous rivulets (Figure 8b). The number of rivulets within the fracture do not increase despite the increasing head from the rising perched water table system. Ceasing the addition of water results in a single continuous rivulet snapping and leaving behind a line of individual static droplets along the path. Sporadic droplet flow continues from the interface along the broken rivulet path, but never fully reconnects the snapped flow path. This continues until all the rivulets present within the fracture snap and no further sporadic droplets occur.

Upon re-addition of water, a single droplet breaches the interface, following the previous flow path of the stationary droplets. This single droplet reconnects all the stationary droplets into a new continuous rivulet. This process repeats itself, reconnecting all the remaining extinct flow paths, while forming no new ones within the fracture. This observation can be attributed to the wettability of material as described by Doe (2001) and emphasises the impact a material's wettability has on variably saturated flow, whereby wetted areas offer less resistance to flow and subsequently will remobilise first.

In the 20g experiment, the number of rivulets present within the fracture increases with the majority of the rivulets occurring as continuous meandering rivulets (Figure 8d). However, discontinuous rivulets with droplet flow were also present in the early stages of wetting. When water supply is stopped, the fracture initially maintains the rivulets. The rivulets continue to drain the overlying material and begin to snap, forming discontinuous rivulets with droplet formation until remnant static droplets persist along the extinct rivulet flow paths. Rewetting of the fracture occurs as the reverse of the drying process, whereby static droplets are remobilised by new droplet formation from discontinuous rivulets until new fully established continuous rivulets are created.

4.2.3. Flow phenomena

Since aperture is constant, the drainage area present within the fracture can be determined by dividing the cumulative rivulet widths by the total fracture width at a specified depth and time after intitial breaching. For example in the 20g experiment, 300 seconds after the intitial breach at 10 mm below the interface, the cumulative rivulet widths is 33 mm and, dividing by the total fracture width of 110

mm, provides a drainage area of 30%. Figure 9 shows the percentage drainage area for the 20g experiment at 10 mm reference depth intervals up to a final depth of 70 mm below the interface. The graph ends 300 seconds after initial breaching due to inability to accurately contrast rivulet widths against the transparent grid.

After the initial breach, there is a rapid increase in drainage area throughout the fracture until approximately 15 (*6000*) seconds; at which stage the drainage area continues to gradually increases until 100 (*40000*) seconds, and a set drainage area is established within the fracture. The upper 50 mm of the fracture shows an average drainage area of 28% while the remaining 20 mm shows an average drainage area of 16%. This decrease of drainage area with depth within a discrete fracture can aid in explaining an observation by Tokunaga et al (2005), where the merging of rivulets within a pile of rocks causes the flow system to change from a disorganised to more organised state. Furthermore, this decreasing drainage area with depth can only be accomodated by an increase in seepage velocity in lower portions of the fracture or, alternatively, an accumulation of excess water elsewhere. The latter is clearly evident from the formation of the dispersion plume along the interface.

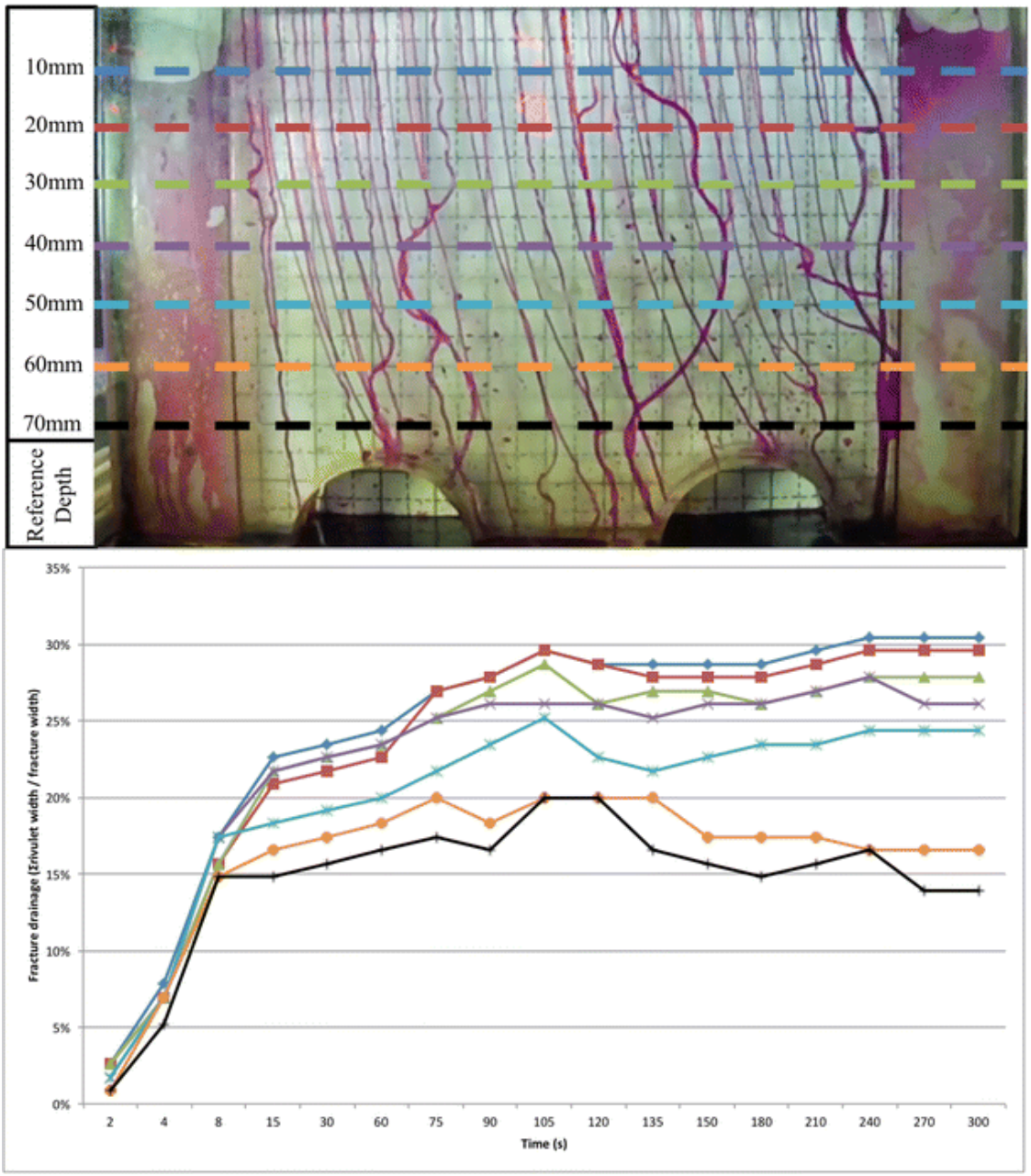

Figure 9 - Fracture drainage area percentage for 20g experiment at 10, 20, 30, 40, 50, 60 and 70 mm reference depths below interface

Ultimately, at 300 seconds, the percentage drainage areas for the 10 mm, 20 mm, 30 mm, 40 mm, 50 mm, 60 mm and 70 mm reference depths are 30%, 30%, 28%, 26%, 24%, 17% and 14% respectively if rivulets span both walls. However, rivulets do not span both walls, as is evident by the continuous 'oscillating' rivulets that transverse freely throughout the fracture while having no influence on the cross cutting continuous rivulets as shown by Figure 10.

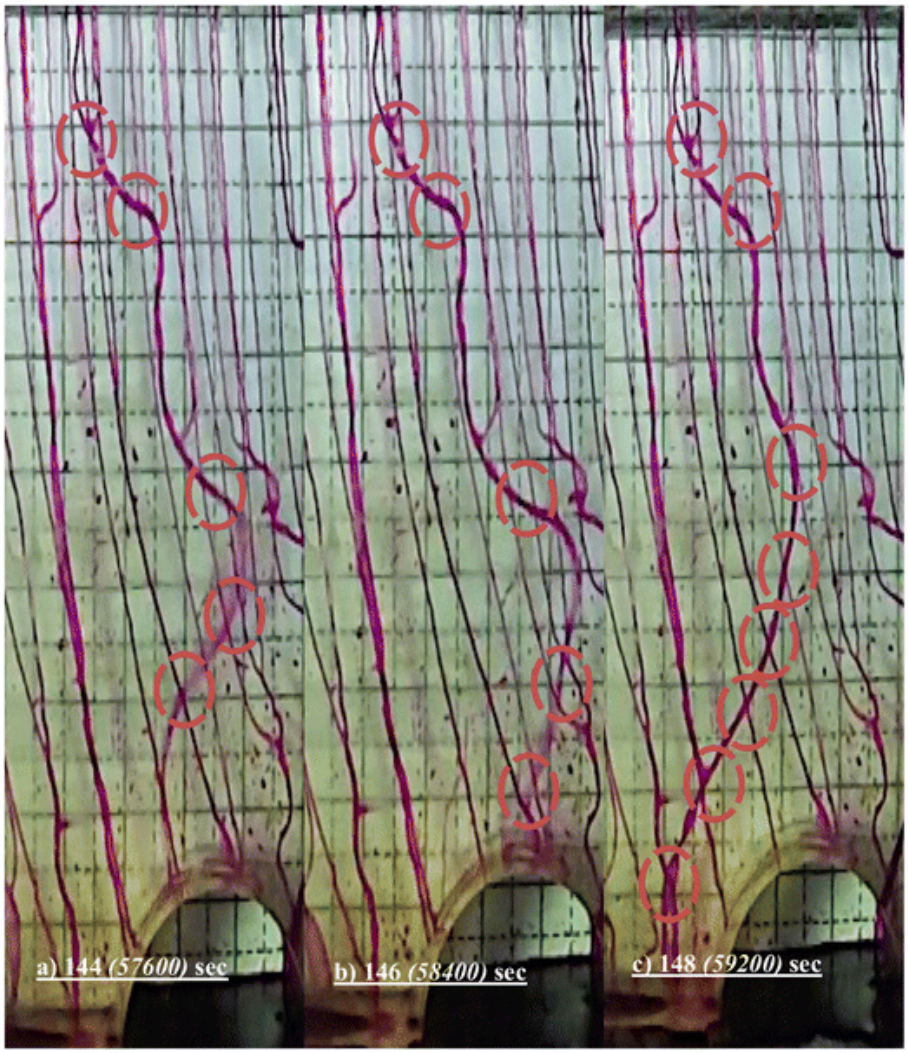

Figure 10 - Fracture view screenshot sequence of cross cutting oscillating rivulets observed in the 20g experiment, with red circles indicating points of no interference.

The intensity of oscillation increases with increasing growth of the saturated wetting front along the interface. This can be attributed to an increased hydraulic gradient and subsequent increase in flow rate through the individual rivulets. Conversely, during the drying cycle, the degree of oscillation decreases until continuous meandering rivulets occur. On occasion, separate oscillating rivulets flowing on the same fracture wall would merge as shown by the circle in Figure 11a-b: the two rivulets connect 25 (*500*) mm below the interface, causing an ejection of droplets at approximately 30-40 (*600-800*) mm below the interface. The majority of ejected droplets drain freely down the fracture while a new flow path is established (Figure 11c-f), where droplets are indicated by arrows and extinct flow paths are shown by dashed lines. The merging of oscillating rivulets in the upper regions of the fracture form fewer main draining continuous meandering rivulets in the lower regions of the fracture. This, in

combination with the observed merging during initial breaching, can explain how the drainage area percentage within the fracture decreases with depth (Figure 9).

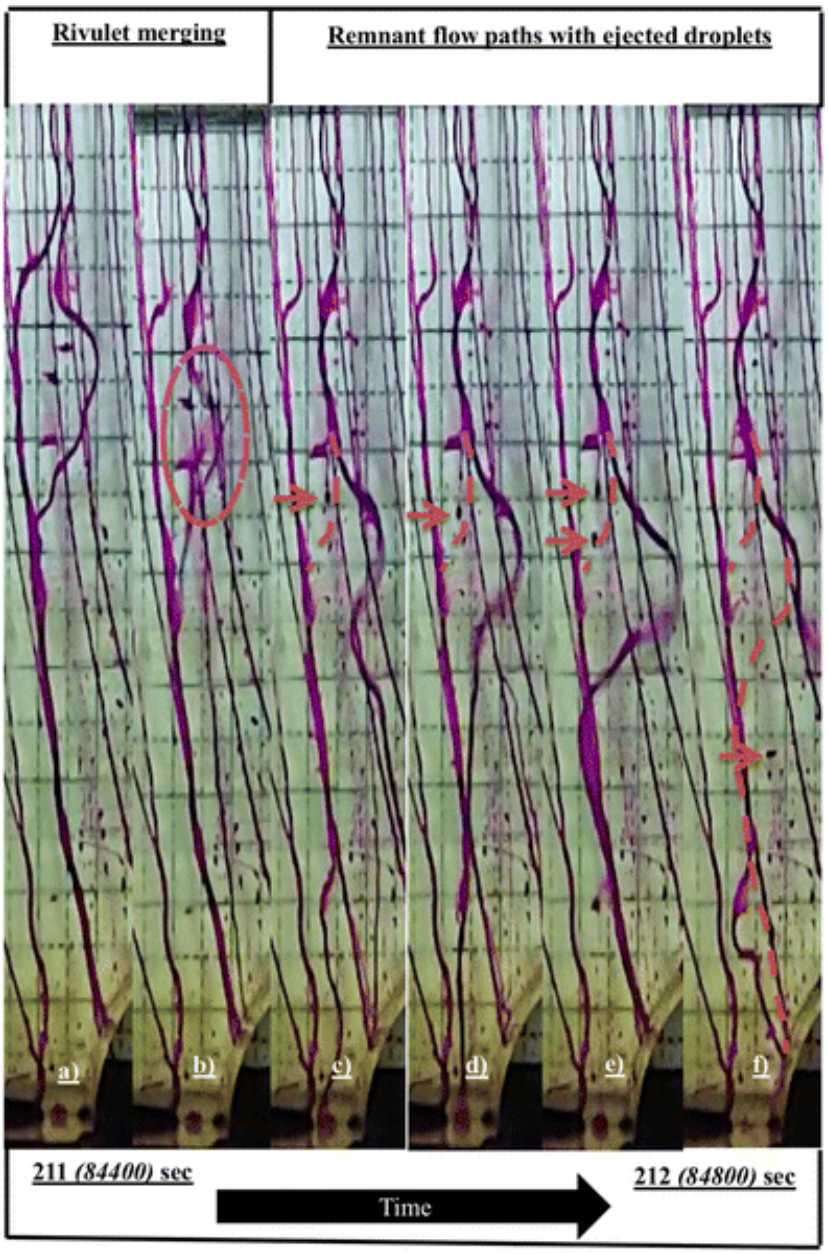

Figure 11 - Fracture view screenshots of merging rivulets progression with arrows showing ejected droplets and dashed lines showing previous flow paths during 20g experiment.

4.3. Findings

The similarity in breaching and flow mechanisms for both acceleration levels supports the findings by Jones et al. (2017a) that the geotechnical centrifuge can be used to observe variably saturated flow

mechanisms and phenomena through fractures as well as account for dispersion in soils. Figure 12 summarises the findings of this research as follows:

(a) Formation of dispersion plume during initial saturation that encounters a capillary barrier at the soil-rock interface;

(b) Combined capillary barrier and multiple flow mechanisms for variably saturated flow at the soil-rock interface;

(c) Final drying phase outcome with invasion of drying plume and static droplets with extinct rivulets in the fracture;

(d) Final rewetting phase outcome with the formation of a rewetting dispersion plume and larger main draining rivulets resulting in decreasing saturation with depth inside the fracture;

(e) Fracture view of initial partial saturation fracture flow mechanisms indicating point sources and oscillating and/or meandering rivulets;

(f) Fracture view of flow phenomenon occurring within partially saturated fractures indicating cross cutting rivulets and merging rivulets.

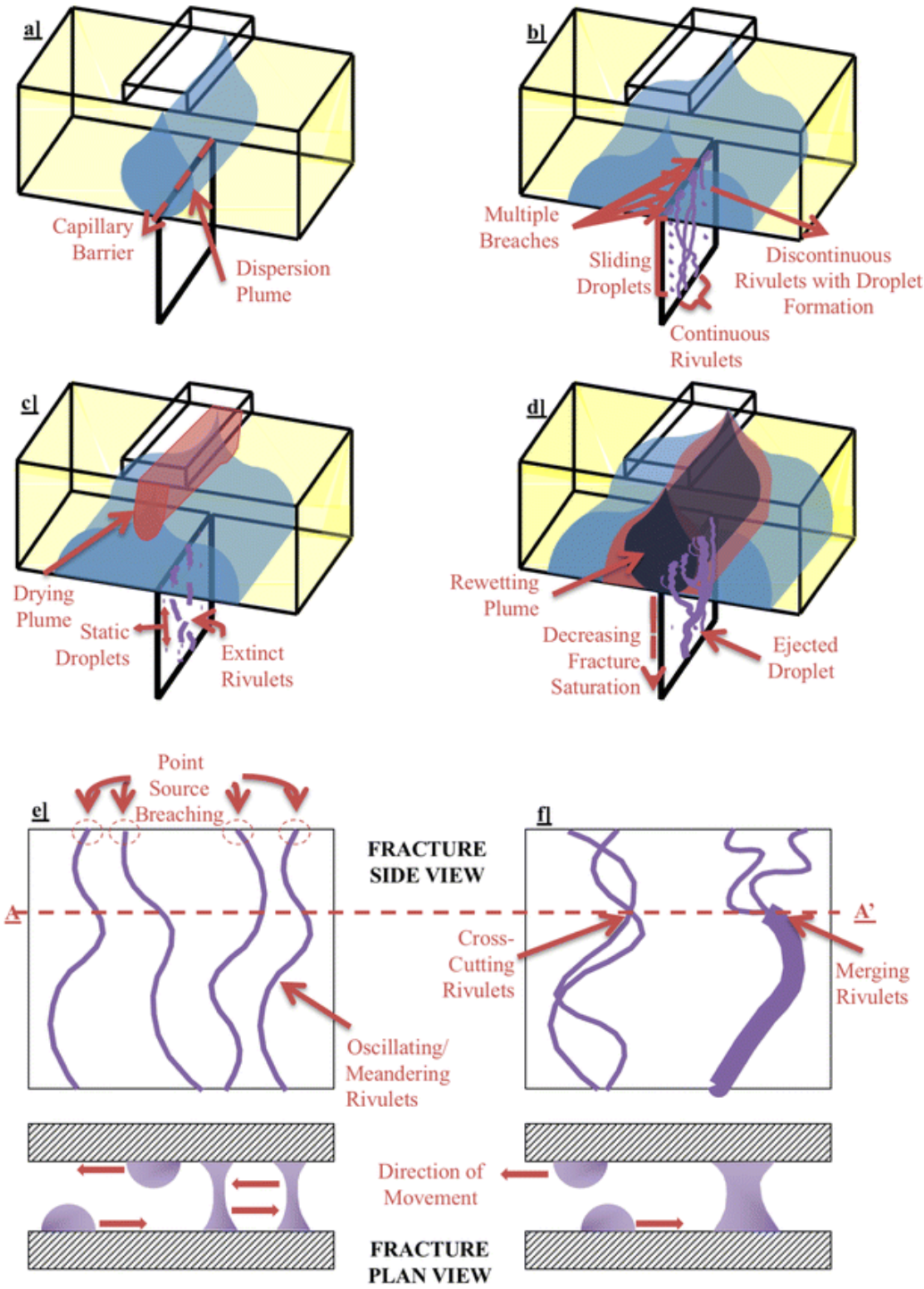

Figure 12: Conceptual model of variable saturated flow from soil into a discrete fracture.

The formation of a bell dispersion plume shape and transverse progression of the saturated wetting front along the interface indicates the pressence of a capillary barrier at the interface. Breaching into the fracture occurs as point sources through the interface, further supporting the capillary barrier

conceptual model and possibility for the overlying material (i.e. saprolite) to hydraulically link the two media and act as preferential flow feeding channels supporting Boisson et al. (2015), Kosugi et al. (2006) and Salve et al. (2012), with fracture seepage velocities dependent on the hydraulical properties of the overlying material and liquid mode within the fracture (Nimmo, 2005). The alternating cycles of wetting and drying (i.e. saturation events) shows the development of multiple dispersion plume stages with each new saturating plume intruding and expanding the previous dispersion plume geometry in a circular and outwards manner. This causes only a small proportion of the original plume to encounter the soil-rock interface indicating the possibility of pollutants and contaminants to be trapped within the soil profile for prolonged periods between saturating events from the omitted plume volume. Within the fracture, new saturation events generally tend to resaturate previous flow paths indicating the importance of the material's wetability, where in more natural conditions a larger wetted surface area can be expected due to the decreased contact angle of rock material and fracture roughness.

Following breaching from sand into the fracture, the flow mechanisms present mimic previous research performed with no overlying material (e.g. Dragila and Weisbrod 2003; Nicholl et al. 1994; Su et al. 1999;), indicating that the current conceptual models, observations and behaviour for unsaturated fracture flow can be extended to the soil-rock interface, supporting the film flow conceptual model. Despite this simplified scenario of sand overlying a vertical fracture, the observed oscillating, meandering, flow-switching and merging of rivulets also occur in more natural conditions, with flow instability caused by the competition between interfacial capillary, gravitational and viscous forces being in similar orders of magnitude, and subsequently causing the flow to exist in near-instability conditions. The decreasing drainage area with fracture depth due to flow instability that causes the merging of rivulets support Jones et al.'s (2017b) findings that vertical fractures do not achieve full saturation in free draining conditions and the current techniques that quantify partially saturated fracture flow are debatable. Although a number of mathematical models attempt to quantify capillary and film flow over a wide range of moisture conditions in soil material (e.g. Lebeau and Konrad 2010; Peters and Durner 2008; Zhang 2011), the more prominent challenge is recording the interaction of film and capillary forces within a fracture. Despite the difficulties and evidence for both conceptual models at the soil-rock interface, an improved understanding of these forces provide an opportunity to

create a combined conceptual model that incorporates multiple flow mechanisms and flow instabilities over a range of media.

5. Conclusion

A series of physical experiments using the geotechnical centrifuge were created to investigate the current conceptual models of partially saturated flow at the soil-rock interface. The model incorporated a clean dry smooth parallel vertical single fracture and results in the dispersion plume forming a bell shape and the development of a saturated wetting front seen from the fracture view at the soil-rock interface supporting the capillary barrier conceptual model. The alternating drying and wetting cycles indicate a potential for pollutants to be trapped above the soil-rock interface as each subsequent saturation event causes the divergence of the previous dispersion plume dimensions. Breaching through the interface displayed identical characteristics for both acceleration levels and occurred as multiple point sources, indicating the overlying material behaves as preferential feeding channels to fractures.

The flow mechanisms encountered within the fracture mimics findings by Nicholl et al. (1994), Dragila and Weisbrod (2003) and Su et al. (1999), where breaches occur as droplets leading to discontinuous meandering rivulets with droplet formation that eventually establish to to a set number of fully sustained continuous rivulets supporting the film flow conceptual model for the soil-rock interface. This similarity of flow mechanisms supports Jones et al (2017a) the geotechnical centrifuge as a tool to observe partially saturated fracture flow in simplified conditions and further implies that the oscillating, meandering, flow-switching and merging of rivulets occur in natural conditions. The merging of oscillating rivulets spanning between both fracture walls in the upper regions of the fracture result in fewer major draining rivulets in the lower regions of the fracture. While evidence of rivulets occurirng separately on both fracture walls, seen by the lack of interference by oscillating cross cutting rivulets, shows that multiple flow mechanisms play significant roles in explaining partially saturated fractures.

Despite the difficulties currently being faced in recording the force interactions governing unsaturated flow, it is an important, developing and current research area in unsaturated fluid mechanics. The contrasting evidence for both conceptual models of the soil-rock interface demonstrate that a combined

conceptual model that incorporates the flow mechanisms and flow instabilities observed in this simplified soil-rock interface model is required for explaining and quantifying numerous characteristic flow features that occur in more complex natural conditions of the fractured vadose zone.

Acknowledgements and Declaration

The authors wish to acknowledge the South African Water Research Commission (www.wrc.org.za) for continuous funding of ongoing research through projects K5/2326 (on the intermediate vadose zone) and K5/2449 (on contaminant transport through the vadose zone from cemetery sites).

Appreciation is also extended to the journal, its editors and reviewers.

The authors declare no conflict of interest.

References

Appels, W.M., Graham, C.B., Freer, J.E., and McDonnell, J.J., (2015). Factors affecting the spatial pattern of bedrock groundwater recharge at the hillslope scale. Hydrological Processes.

Archer, A., (2014). 'Using Small-strain stiffness to predict the settlement of shallow foundations on sand'. Meng (Geotechnical Engineering) dissertation, University of Pretoria, Pretoria, South Africa.

Banks, E.W., Simmons, C.T., Love, A.J., Cranswick, R., Werner, A.D., Bestland, E.A., Wood, M., and Wilson, T., (2009). Fractured bedrock and saprolite hydrogeologic controls on groundwater/surface-water interaction: a conceptual model (Australia). Hydrogeology Journal, 17(8):1969-1989.

Boisson, A., Guihéneuf, N., Perrin, J., Bour, O., Dewandel, B., Dausse, A., Viossanges, M., Ahmed, S., and Maréchal, J.C., (2015). Determining the vertical evolution of hydrodynamic parameters in weathered and fractured south Indian crystalline-rock aquifers: insights from a study on an instrumented site. Hydrogeology Journal, 23(4):757-773.

Butterfield, R., (2000). Scale-modelling of fluid flow in geotechnical centrifuges. Soils and foundations, 40(6):39-45.

Buttle, J.M., and mcdonald, D.J., (2002). Coupled vertical and lateral preferential flow on a forested slope. Water Resources Research, 38(5):18-1.

Culligan-Hensley, P. J. & Savvidou, C. (1995). Environmental geomechanics and transport processes. In: R. Taylor, ed. Geotechnical Centrifuge Technology. Blackie Academic and Professional, Glasgow, pp. 196-264.

Culligan, P.J. and Barry, D.A., (1998). Similitude requirements for modelling NAPL movement with a geotechnical centrifuge. PROCEEDINGS-INSTITUTION OF CIVIL ENGINEERS GEOTECHNICAL ENGINEERING, pp.180-186.

Della Volpe, C., Maniglio, D., Morra, M. and Siboni, S., (2002). The determination of a 'stable-equilibrium' contact angle on heterogeneous and rough surfaces. Colloids and Surfaces A: Physicochemical and Engineering Aspects, 206(1):47-67.

Dippenaar, M. A. (2014a). Towards hydrological and geochemical understanding of an ephemeral palustrine perched water table "wetland" (Lanseria Gneiss, Midrand, South Africa). Environmental Earth Science. 72(7):2447-2456.

Dippenaar, M. A. (2014b). Porosity reviewed: quantitative multi-disciplinary understanding, recent advances and applications in vadose zone hydrology. Geotechnical and Geological Engineering. 32:1-19.

Dippenaar, M. A. and Van Rooy, J. L. (2016). On the cubic law and variably saturated flow through discrete open rough-walled discontinuities. Int. J. Rock Mech. Min. Sci. 89:200-211.

Doe, T.W., (2001). What do drops do? Surface wetting and network geometry effects on vadose-zone fracture flow in CONCEPTUAL MODELS OF FLOW AND TRANSPORT IN THE FRACTURED VADOSE ZONE, pp 243-270.

Dragila, M.I., and Weisbrod, N., (2003). Parameters affecting maximum fluid transport in large aperture fractures. Advances in water resources, 26(12):1219-1228.

Dragila, M.I., and Wheatcraft, S.W., (2001). Free-surface films in CONCEPTUAL MODELS OF FLOW AND TRANSPORT IN THE FRACTURED VADOSE ZONE, pp 217-241.

Faybishenko, B., Doughty, C., Steiger, M., Long, J.C., Wood, T.R., Jacobsen, J.S., Lore, J., and Zawislanski, P.T., (2000). Conceptual model of the geometry and physics of water flow in a fractured basalt vadose zone. Water Resources Research, 36(12):3499-3520

Fujimoto, M., Kosugi, K.I., Tani, M., Banba, N., and Fukagawa, R., (2014). Evaluation of Bedrock Groundwater Movement in a Weathered Granite Hillslope Using Tracer Methods. International Journal of Erosion Control Engineering, 7(1):32-40.

Garnier, J., Gaudin, C., Springman, S. M., Culligan, P. J., Goodings, D. J., Konig, D., Kuttervii, B., Phillips, R., Randolph, M.F., and Thorel, L., (2007). Catalogue of scaling laws and similitude questions in geotechnical centrifuge modelling. International Journal of Physical Modelling in Geotechnics, 7(3):1-23.

Ghezzehei, T.A., (2004). Constraints for flow regimes on smooth fracture surfaces. Water resources research, 40(11).

Graham, C.B., Woods, R.A., and McDonnell, J.J., (2010). Hillslope threshold response to rainfall:(1) A field based forensic approach. Journal of Hydrology, 393(1):65-76.

Hsieh, P.A., Bahr, J.M., Doe, T.W., Flint, A.L., Gee, G., Gelhar, L.W., Solomon, D.K., van Genuchten, M., and Wheatcrsaft, S.W., (2001). Panel Report in CONCEPTUAL MODELS OF FLOW AND TRANSPORT IN THE FRACTURED VADOSE ZONE. Pp 9- 44

Huang, X., Shi, Z.H., Zhu, H.D., Zhang, H.Y., Ai, L., and Yin, W., (2015). Soil moisture dynamics within soil profiles and associated environmental controls. CATENA.

Jones, B. R., Brouwers, L. B., van Tonder, W. D. and Dippenaar, M. A. (2017a). Assessing geotechnical centrifuge modelling in addressing variably saturated flow in soil and fractured rock. Environmental Science and Pollution Research. DOI: 10.1007/s11356-016-8333-2.

Jones, B. R., Brouwers, L. B. and Dippenaar, M. A. (2017b). Partially to fully saturated flow through smooth, clean, open fractures: qualitative experimental studies. Hydrogeology Journal. DOI: 10.1007/s10040-017-1680-3.

Kaytech. (2014). BIDIM Technical Data Sheet with new SANS Standards. Ref DS FLTR 0587-08/2014

Kordilla, J., Tartakovsky, A.M. and Geyer, T., (2013). A smoothed particle hydrodynamics model for droplet and film flow on smooth and rough fracture surfaces. Advances in Water Resources, 59:1-14.

Kosugi, K.I., Katsura, S.Y., Katsuyama, M., and Mizuyama, T., (2006). Water flow processes in weathered granitic bedrock and their effects on runoff generation in a small headwater catchment. Water Resources Research, 42(2).

Kumar, P. R., (2007). Scaling laws and experimental modelling of contaminant transport mechanism through soils in a geotechnical centrifuge. Geotechnical and Geological Engineering, 25(5):581-590.

Lebeau, M. and Konrad, J.M., (2010). A new capillary and thin film flow model for predicting the hydraulic conductivity of unsaturated porous media. Water Resources Research, 46(12).

Liang, W.L., and Uchida, T., (2014). Effects of topography and soil depth on saturated-zone dynamics in steep hillslopes explored using the three-dimensional Richards' equation. Journal of Hydrology, 510:124-136.

Masaoka, N., Yamakawa, Y., Kosugi, K. I., Mizuyama, T., and Tsutsumi, D., (2010). Intensive measurements of soil pore water pressure for analyzing heterogeneous hydrological processes on a hillslope. International Journal of Erosion Control Engineering, 3(1):53-58.

Nimmo, J.R., (2005)., Unsaturated Zone Flow Processes, in Anderson, M.G., and Bear, J., eds., ENCYCLOPEDIA OF HYDROLOGICAL SCIENCES: PART 13--GROUNDWATER: Chichester, UK, Wiley, 4:2299-2322

Nimmo, J.R., (2010). Theory for source-responsive and free-surface film modeling of unsaturated flow. Vadose Zone Journal, 9(2):295-306.

Or, D., (2008). Scaling of capillary, gravity and viscous forces affecting flow morphology in unsaturated porous media. Advances in water resources, 31(9):1129-1136.

Or, D., and Ghezzehei, T.A., (2007). Traveling liquid bridges in unsaturated fractured porous media. Transport in porous media, 68(1):129-151.

Or, D., and Tuller, M., (2000). Flow in unsaturated fractured porous media: Hydraulic conductivity of rough surfaces. Water Resources Research, 36(5):1165-1177.

Peters, A. and Durner, W., (2008). A simple model for describing hydraulic conductivity in unsaturated porous media accounting for film and capillary flow. Water resources research, 44(11).

Phillips, R., (1995). Chapter 3 - Centrifuge medelling: practical considerations IN Taylor, R. E. (Ed.). Geotechnical centrifuge technology. CRC Press.

Salve, R., Rempe, D.M., and Dietrich, W.E., (2012). Rain, rock moisture dynamics, and the rapid response of perched groundwater in weathered, fractured argillite underlying a steep hillslope. Water Resources Research, 48(11).

Singhal, B.B.S., and Gupta, R.P., (2010). Applied hydrogeology of fractured rocks. Springer Science and Business Media.

Sohrt, J., Ries, F., Sauter, M., and Lange, J. (2014). Significance of preferential flow at the rock soil interface in a semi-arid karst environment. Catena, 123:1-10.

Su, G.W., Geller, J.T., Pruess, K., and Wen, F., (1999). Experimental studies of water seepage and intermittent flow in unsaturated, rough-walled fractures. Water resources research, 35(4):1019-1037.

Taylor, R.N., (1995). Chapter 2 - Centrifuges in modeling: Principles and scale effects IN Taylor, R. E. (Ed.). Geotechnical centrifuge technology. CRC Press.

Tokunaga, T.K., and Wan, J., (1997). Water film flow along fracture surfaces of porous rock. Water Resources Research, 33(6):1287-1295.

Tokunaga, T.K., and Wan, J., (2001). Approximate boundaries between different flow regimes in fractured rocks. Water Resources Research, 37(8), pp 2103-2111.

Tokunaga, T.K., Olson, K.R. and Wan, J., (2005). Infiltration flux distributions in unsaturated rock deposits and their potential implications for fractured rock formations. Geophysical research letters, 32(5).

Tuller, M. And Or, D., (2002). Unsaturated hydraulic conductivity of structured porous media. Vadose Zone Journal, 1(1):14-37.

Van Tonder, W.D. & Jacobsz, S.W., (1997). Seepage column hydraulic conductivity tests in the geotechnical centrifuge. Journal of the South African Institution of Civil Engineering, 59(3):16-24.

Wang, J.S.Y. & Narasimhan, T.N., (1993). Unsaturated flow in fractured porous media in FLOW AND CONTAMINANT TRANSPORT IN FRACTURED ROCK, pp. 325-391.

Zhang, Z.F., (2011). Soil water retention and relative permeability for conditions from oven-dry to full saturation. Vadose Zone Journal, 10(4):1299-1308.